REPORT DOCUMENTATION PAGE

Form Approved OMB No. 0704-0188

1. REPORT DATE *(DD-MM-YYYY)*	2. REPORT TYPE	3. DATES COVERED *(From – To)*
07-04-2003	Final Report	1 April 2002 - 01-Jan-03

4. TITLE AND SUBTITLE

INFLUENCE OF LCF LOADINGS ON HCF CRACK GROWTH

5a. CONTRACT NUMBER
F61775-02-WE007

5b. GRANT NUMBER

5c. PROGRAM ELEMENT NUMBER

6. AUTHOR(S)

Professor James Byrne

5d. PROJECT NUMBER

5d. TASK NUMBER

5e. WORK UNIT NUMBER

7. PERFORMING ORGANIZATION NAME(S) AND ADDRESS(ES)

University of Portsmouth
Anglesea Building, Anglesea Road
Portsmouth PO1 3DJ
United Kingdom

8. PERFORMING ORGANIZATION REPORT NUMBER

N/A

9. SPONSORING/MONITORING AGENCY NAME(S) AND ADDRESS(ES)

EOARD
PSC 802 BOX 14
FPO 09499-0014

10. SPONSOR/MONITOR'S ACRONYM(S)

11. SPONSOR/MONITOR'S REPORT NUMBER(S)
SPC 02-4007

12. DISTRIBUTION/AVAILABILITY STATEMENT

Approved for public release; distribution is unlimited.

13. SUPPLEMENTARY NOTES

20030610 223

14. ABSTRACT

This report results from a contract tasking University of Portsmouth as follows: The contractor will conduct an experimental program to examine the effects of low cycle fatigue (LCF) loading on high cycle fatigue (HCF) crack growth. The project will also extend and refine the current model of combined LCF/HCF fatigue crack growth. The project will use Ti-6Al-4V alloy and corner notched specimens for the combined LCF/HCF testing. The program will focus on three main aspects of the problem: 1) Investigate the effect of LCF overloads on larger number of blocks of HCF cycles than previously used, e.g. 10,000/block versus 1,000/block. 2) Introduce overloads into simple spectrum loading. 3) Extend previous modeling of combined cycle fatigue crack growth based on the results of this project.

15. SUBJECT TERMS

EOARD, Metals & alloys, Fatigue, Failure Mechanisms

16. SECURITY CLASSIFICATION OF:			17. LIMITATION OF ABSTRACT	18. NUMBER OF PAGES	19a. NAME OF RESPONSIBLE PERSON
a. REPORT	b. ABSTRACT	c. THIS PAGE			Charles H. Ward, Lt Col, USAF
UNCLAS	UNCLAS	UNCLAS	UL	26	19b. TELEPHONE NUMBER *(Include area code)* +44 (0)20 7514 3154

UNIVERSITY OF PORTSMOUTH

US AFOSR Study Report

The effects of LCF loadings on HCF crack growth

Final Report for F61775-02-WE007

F573

Submitted by:

R.F. Hall, J. Ding and J. Byrne

February 2003

MECHANICAL BEHAVIOUR OF MATERIALS LABORATORY

DEPARTMENT OF MECHANICAL AND DESIGN ENGINEERING

Anglesea Building, Anglesea Road
Portsmouth PO1 3DJ

Phone: +44 (0)23 92 842370 E-mail: jim.byrne@port.ac.uk
Phone: +44 (0)23 92 842325 E-mail: rod.hall@port.ac.uk
Fax: +44 (0)23 92 842351

Signed statement for final report for EOARD contract SPC 024007

I.
In accordance with Defence Federal Acquisition Regulation 252.227-7036, Declaration of Technical Data Conformity Jan 1997), the contractor, University of Portsmouth, hereby declares that, to the best its knowledge and belief, the technical data delivered herewith under Contract No. F61775-02- WE007 is complete, accurate and complies with all requirements of the contract.

II.
In accordance with the requirements in Federal Acquisition Regulation 52.227-13 Patent Rights- Acquisition by the U.S. Government (Jun 1999): a) Disclosure of all subject inventions as defined in FAR 52.227-13 have been reported in accordance with this clause b) I certify that there were no subject inventions to declare as defined in FAR 52.227-13, during the performance of this contract.

Signed. J Byrne (Prof. J. Byrne)
1/4/03.

THE EFFECT OF LCF LOADINGS ON HCF CRACK GROWTH

REPORT FOR THE PERIOD to February 2003

REPORT NO F 573

NOTATION

CN	corner notched
DCPD	direct current potential difference
FCG	fatigue crack growth
FOD	foreign object damage
HCF	high cycle fatigue
LCF	low cycle fatigue
MOC	multiple overload cycles: a type of HCF + LCF loading
MUC	multiple underload cycles: a type of HCF + LCF loading
SOC	single overload cycle: a type of HCF + LCF loading
SUC	single underload cycle: a type of HCF + LCF loading
da/dN_{HCF}	crack growth increment resulting from the application of a HCF cycle
da/dN_{LCF}	crack growth increment resulting from the application of a LCF cycle
da/dB	crack growth increment resulting from the application of a HCF + LCF loading block
da/dB_{HCF}	crack growth increment resulting from the application of the HCF cycles within a loading block
da/dB_{LCF}	crack growth increment resulting from the application of the LCF cycles within a loading block
ΔK, DK	stress intensity range
ΔK_{HCF}	stress intensity range associated with a HCF cycle
ΔK_{LCF}	stress intensity range associated with a LCF cycle, i.e. the peak-to-peak load cycle
$\Delta K_{HCF,onset}$	the value of ΔK_{HCF} associated with the onset of HCF crack growth
$\Delta K_{LCF,onset}$	the value of ΔK_{LCF} associated with the onset of HCF crack growth
ΔK_{th}	threshold value of stress intensity range
$K_{max,th}$	threshold value of maximum stress intensity
$\sigma_{max,HCF}$	maximum HCF stress
$\sigma_{min,HCF}$	minimum HCF stress
$\sigma_{max,LCF}$	maximum LCF stress
$\sigma_{min,LCF}$	minimum LCF stress
N_{HCF}	number of HCF cycles in a loading block
N_{LCF}	number of LCF cycles in a loading block
n	ratio N_{HCF} : N_{LCF}
R_{HCF}	stress ratio of the HCF cycles
R_{LCF}	stress ratio of the LCF cycles
s	seconds
T	overload ratio; i.e. the maximum LCF stress / maximum HCF stress.
W	Wheeler constant

3. INTRODUCTION

A current design limitation for aero-engine discs and fan blades is that of the material's resistance to low cycle fatigue (LCF). In such rotating components the LCF loading arises from the cyclic

variation of both the centrifugal and the thermal stresses. In the simplest case this substantial stress variation occurs once per flight. However, rotating engine components may also experience high cycle fatigue (HCF) failures as a direct result of excessive vibrational stresses. Consequently, in order that the fatigue integrity of these critical rotating components might be fully assessed, it is necessary to establish the resistance of the disc or fan blade material to the conjoint action of HCF and LCF loadings.

When HCF and LCF cycles are conjointly applied, initially at low values of ΔK, the HCF cycles are not effective. However, at a value of ΔK dependent on factors such as the material being tested and load levels of both LCF and HCF cycles, the HCF cycles commence to contribute to the overall FCG rate. With a large number of HCF cycles compared to LCF cycles, this point usually signifies the end of useful life. The effect is schematically presented in Figure **1**, where ΔK_{onset} is the point at which the HCF cycles become effective.

This report extends our previous work **[1-4]** with combined HCF+LCF cycles at a stress ratio of 0.9 and using a cycle ratio of 10 000 HCF cycle to 1 LCF cycle. The representations of the loading waveforms are illustrated in Figure **2**. Those used for experiments covered by this report are single underload cycles and single overload cycles. Further threshold tests have been carried out both without overloads and including LCF overload prior to the application of HCF cycles, Figure **3**. It has not been possible to conduct experiments where specific overloads are introduced into a spectrum loading, as initially proposed. However, the modelling of single overloads on HCF+LCF has been extended to use the FASTRAN software, developed by Newman **[5]**

2. EXPERIMENTAL PROCEDURE

The present work is concerned to measure and model the fatigue crack growth (FCG) rates associated with HCF loadings, particularly as they are affected by the presence of different proportions of LCF induced fatigue crack growth. The threshold values for HCF crack growth, both in the presence and absence of LCF crack growth, are studied, since they may be used to calculate critical crack sizes for components and structures subjected to HCF stress cycles.

Corner notched specimens of forged Ti-6Al-4V have been cyclically loaded in a special test facility which combines an electromagnetic vibrator with a servo-hydraulic fatigue machine. This hybrid machine can therefore apply HCF cycles and LCF cycles either separately or conjointly. The HCF cycles are of sinusoidal form and the LCF cycles are trapezoidal

A pulsed direct current potential difference (DCPD) system has been used to monitor crack growth. Voltage readings from the notch of the specimen and at a remote reference point have been measured by a multimeter with a resolution of 0.001mV and automatically downloaded onto a computer spreadsheet. Analysis of the test results is presented as diagrams of FCG rate, da/dN, by the 3-point secant method, against ΔK calculated using Pickard's **[6]** solution for CN type specimens.

3. EXPERIMENTAL RESULTS

3.1 INCREASED HCF+LCF CYCLE RATIO

In a previous report **[4]** it was shown that at a stress ratio of 0.9, the effect of overloads on the contribution of HCF cycles to overall HCF+LCF was indeterminate, Figure **4**. It was noted however that the use of only 1000 HCF cycles with 1 LCF cycle could be inadequate and that the use of a larger number, e.g. 10 000 HCF cycles to 1 LCF cycle could provide more information. The effect on experimental work of using this increased cycle ratio is that the time taken for each experiment is increased roughly in proportion to the number of HCF cycles.

Results from two experiments at R=0.9 using a cycle ratio of 10 000:1 and without overload have been completed, Figure **5**. It is seen that the increase in HCF cycles has had the desired result in that a clear onset of HCF contribution to crack growth is observed and above onset, FCG rates are mostly outside the LCF scatterband which has been used as the guide to determine if suppression of HCF cycle contribution to crack growth has occurred. The disparity between the two sets of data is not important in the present context, the objective being to demonstrate a definite contribution by HCF cycles to overall crack growth which both experiments clearly show. Having demonstrated an HCF contribution to crack growth, the amount of overload to suppress this needs to be found.

Two further experiments at R=0.9 and cycle ratio 10 000:1 have been undertaken, but this time with an overload of 30% i.e. an overload ratio of T=1.3. The results of these experiments are presented in Figure **6**. The majority of the data falls within the LCF only scatterband and therefore it can be stated that an overload of 30% prior to the application of 10 000 HCF cycles at a stress ratio of 0.9 effectively suppresses the damaging influence of the HCF cycles.

In both experiments, the last couple of data points are above the upper bound of scatter in LCF data and an equal number are below the lower bound at a little smaller ΔK value. A tendency for data to be erratic near the end of an experiment has been observed before **[3 & 4]** and is regarded as inconsequential in the analysis of the principal features in HCF+LCF crack growth. The experimental data above the LCF scatterband does not indicate an onset of HCF activity because although the onset of HCF cycles damage has been found to increase by the application of prior LCF overloads the difference between the mean value of 22 MPa$\sqrt{m}$ without overload and approximately 34 MPa$\sqrt{m}$ with 30% overload is too great.

Although an overload of 30% definitely suppresses the HCF cycle contribution to crack growth, it has not been possible to determine whether a smaller overload would achieve the same objective. It has also not been possible to follow the logical progression, by investigating overloads necessary to suppress HCF cycle activity resulting from larger cycle ratios such as 100 000:1.

3.2 INFLUENCE OF OVERLOADS ON HCF THRESHOLD

Further threshold experiments have been undertaken and the results are presented in Figure **7.** Unfortunately a completely logical pattern does not emerge. At T=0.8 the value of ΔK_{th} for T=1.3 is high in relation to T = 1.75 and T=2.0 but at R=0.7 it is low in relation to T =1.0. In addition the value for T=1.75 at R=0.8 is low in relation to T = 1.0. The reason for these anomalies is not known at present. Although specimens from different batches of material were used in the experiments, this does not appear to be the reason for the inconsistencies.

However, certain trends can be observed. At the high stress ratio of R=0.9, overloads have little effect on the value of ΔK_{th}; the mean values range from 2.2 to 2.3 MPa$\sqrt{m}$. The influence of overloads increases as the stress ratio is reduced. At R=0.8 there appears to be some effect on the

value of ΔK_{th}, ranging from 2.6 to 3.2 MPa$\sqrt{m}$, but at R=0.7 the effect is clear, with ΔK_{th} ranging from 2.8 to 4.3 MPa$\sqrt{m}$. As is to be expected, prior LCF overloads increase the value of ΔK_{th}, the greater the overload, the greater the increase.

4. CRACK GROWTH MODELLING

This study employs the FASTRAN code to predict crack growth behaviour under a range of major/minor cyclic combinations with the effect of overload. FASTRAN, developed by Newman **[7]**, is based on a strip-yield model **[8]** but modified to leave plastically deformed material in the wake of a crack. It also attempted to model three-dimensional effects by employing a constraint factor, α, which is used to elevate the flow stress at the crack tip to account for the influence of stress rate. The details of the model are given elsewhere **[5 & 7]** and are simply summarized in Appendix A. In the past two decades FASTRAN has been shown capable of predicting crack growth behaviour of a series of Aluminium alloys under complex loading conditions **[9-11].**

To make a life prediction using FASTRAN, the curve of FCG rate (da/dN) versus effective stress intensity factor range ΔK_{eff} is required as input. In the present study, this curve is estimated from FCG rate against stress intensity range (ΔK) data under constant-amplitude HCF loadings with high stress ratios, since in such conditions the plasticity-induced closure effect is considered to be negligible and ΔK can be approximately regarded as ΔK_{eff}. The da/dN against ΔK curves under HCF loadings only, with stress ratios of 0.7 and 0.8, have been reported before **[1-4]** and are shown in Figure 8. Obviously, due to the absence of closure effects, the FCG rate is independent of R for rates greater than 1×10^{-10} m/cycle. A difference is however observed in the near-threshold regime, where the threshold value at the stress ratio of 0.7 is higher than that at the stress ratio of 0.8. It may be interpreted by the influence of other closure effects at this regime, such as roughness- and oxide- induced closure **[11]**, particularly at the lower stress ratio (i.e. R=0.7), or an intrinsic mean stress intensity effect. Accordingly, the da/dN and ΔK_{eff} relation at the low rate regime is assumed to be close to the data for the stress ratio of 0.8. The solid line, as shown in Figure 8, is finally used to represent the relationship between da/dN and ΔK_{eff}.

Apart from the relation of da/dN and ΔK_{eff}, the effective threshold $(\Delta K_{eff})_{th}$ as a function of stress ratio is also required by FASTRAN. Newman argued that the effective thresholds should be

lower than the corresponding large-crack experimental data. The $(\Delta K_{eff})_{th}$ versus R curve is therefore estimated as illustrated in Figure 9, with comparison of the measured threshold values under HCF loadings only.

In terms of inputs, FASTRAN is used to predict the ΔK against da/dN curves under various stress ratios and overload ratios. Figures 10 and 11 show the change of predicted ΔK- da/dN curve with overload ratios from 1.0 to 2.0 or 1.45, under stress ratios of 0.7 and 0.8, respectively. The corresponding experimental data are also included in the figures for comparison. Considering the scatter of fatigue tests, the predicted curves are in reasonable agreement with experimental data.

From Figures 10 and 11, it is also seen that FASTRAN can predict the onset point (ΔK_{onset}) for combined HCF and LCF loading, beyond which HCF loading begins to contribute to the growth. Further cases have been investigated, and the comparison of predicted and experimental onset points is illustrated in Figure 12. For all cases the difference between the prediction and measured value is well within ±20%.

In summary, FASTRAN, which uses a plasticity-induced closure model to simulate the retardation phenomenon caused by overload, predicted well crack growth rate data on forged Ti-6Al-4V under LCF and HCF loading combinations for a wide range of stress ratios and overload ratios. FASTRAN also predicted the transition of onset point due to the effect of overload. As a fatigue crack growth prediction code, FASTRAN is easy to use since input data required can be obtained via constant-amplitude fatigue loadings, as described earlier.

Accuracy of predictions, especially for the ΔK_{onset} point, needs to be further improved. To do this, future work should address: (a) crack growth rate over the widest possible range (from threshold to fracture) under high stress-ratio HCF loadings, to accurately capture the relationship between effective stress intensity range and growth rate; (b) the relationship between effective threshold and large-crack threshold, to obtain the correct effective threshold versus stress ratio curve. The latter work is assumed to be significantly important for the determination of the onset point.

5. CONCLUSIONS

1. At a stress ratio of 0.9, an increase in the cycle ratio used for experiments, from 1000:1 to 10 000:1, results in a clear onset of HCF contribution to crack growth.

2. A prior LCF overload of 30 % effectively suppresses the HCF contribution to crack growth at R=0.9 at the cycle ratio of n=10 000:1.

3. The application of prior LCF overloads has little influence on threshold values at a stress ratio of R=0.9 but a significant increase in threshold is observed, dependent on overload ratio, at lower stress ratio of R=0.8 and 0.7.

4. The application of the FASTRAN code has predicted quite well both the FCG rates observed experimentally and the ΔK_{onset} values at which HCF cycles begin to contribute to crack growth. However, some refinement of input data is still required in terms of effective stress intensity range and threshold values.

5. FUTURE WORK

1. The work on the influence of LCF overloads on fatigue crack growth rates under combined HCF+LCF will be extended to 350^0C under an I.R.I. research grant, contract F61775-00-WE041, (2003/2004).
2. Under a U.K. EPSRC/MOD award, the influence of FOD on FCG under combined HCF+LCF will be investigated (2002/2004).

REFERENCES

[1] Hall, R.F., & Powell, B.E. US AFOSR Study Report; Annual Report for Phase II, **F567**, May 1999

[2] Hall, R.F., Powell, B.E. & Byrne, J. US AFOSR Study Report; Interim Report for Phase III, **F568**, November 1999

[3] Hall, R.F., Powell, B.E. & Byrne, J. US AFOSR Study Report; Annual Report for Phase III, **F569**, October 2000

[4] Hall, R.F., Powell, B.E. & Byrne, J. US AFOSR Study Report; Interim Report for Phase IV, **F570**, May 2001

[5] Pickard, A.C. "The application of 3-dimentional finite element methods to fracture mechanics and fatigue life predictions" EMAS, 1986..

[6] J. C., Jr. Newman, "FASTRAN II - a fatigue crack growth structural analysis program," NASA TM 104159, 1992.

[7] J. C., Jr. Newman, "A crack-closure model for predicting fatigue crack growth under aircraft spectrum loading," Methods and Models for Predicting Fatigue Crack Growth under Random Loading, ASTM STP 748, 1981, 53-84.

[8] D. S. Dugdale, "Yielding of steel sheets containing slits," J. Mech. Phys. Solids 8, 1960, 100-104.

[9] J. C., Jr. Newman & P. R. Edwards, "Short-crack growth behaviour in an aluminum alloy - an AGARD cooperative test programme," AGARD R-732. 1988.

[10] J. C., Jr. Newman, " Effects of constraint on crack growth under aircraft spectrum loading," A. Beukers et al. (eds), Fatigue of Aircraft Materials, Delft University Press, 1992, 83-109.

[11] J. C., Jr. Newman, " Crack growth under variable amplitude and spectrum loading in 2024-T3 aluminum alloys", Proceedings of the TMS Fall Meeting, 1997, 109-121.

[12] J. C., Jr. Newman, "A crack-opening stress equation for fatigue crack growth," Int. J. Fracture, 1984, R131-R135.

[13] W. Elber, "The significance of fatigue crack closure," Damage Tolerance in Aircraft Structures. ASTM STP 486, 1971, 230-242.

Appendix A. FASTRAN model and crack growth equation

The model was based on the Dugdale strip-yield model **[8],** but modified to make the wake of the crack described by elastic-plastic elements. Thus the plastic-zone size and crack-surface displacement are obtained by superimposing two elastic problems: (a) a crack in a finite-width plate subjected to remote uniform stress, *S*, and (b) to a uniform stress, σ, applied over a segment of the crack surface.

Figure **A.1** shows a schematic diagram of the model at maximum and minimum applied stresses. The model is composed of three regions: (1) a linear elastic region containing a fictitious crack of half length $c+\rho$, (2) a plastic region of length ρ, and (3) a residual plastic deformation region along the crack surfaces. The physical crack is of half-length c-r, where r is the radius of the hole. The compressive plastic zone is ω. Regions 2 and 3 are composed of rigid-perfectly plastic (constant stress) bar elements with a flow stress σ_0.

At any applied stress level, the bar elements are either intact (in the plastic zone) or broken (residual plastic deformation). The broken elements carry compressive loads only, and then only if they are in contact. At the maximum applied stress and when the crack is fully open, the effects of stress state on plastic zone size and displacements are approximately accounted for by using a constraint factor α. Thus, although the strip-yield model does not model the correct yield-zone shape for plane-strain conditions, the model with a high constraint factor is able to produce crack-surface displacement and crack-opening stresses quite similar to those calculated from three-dimensional, elastic-plastic, finite-element analyses of crack growth and closure for finite-thickness plates. At the minimum applied stress, some elements in the plastic zone and elements along the crack surface that are in contact may yield in compression when the contact or compressive stress reach $-\sigma_0$.

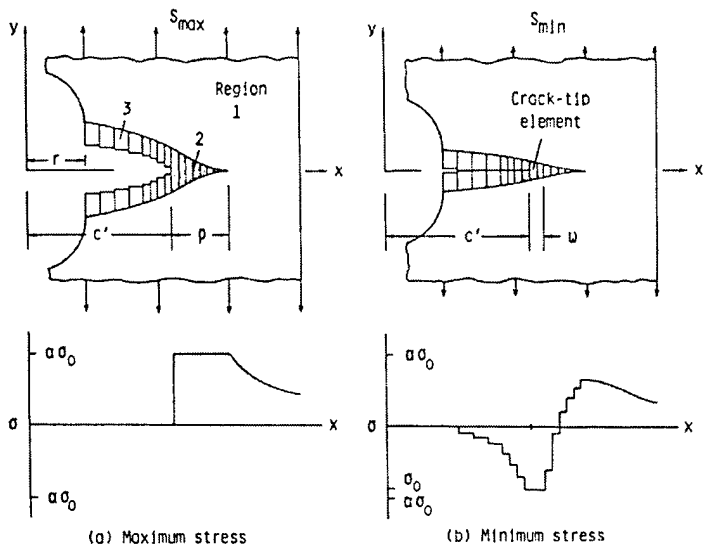

Figure A.1

The above analytical crack-closure model was used to calculate crack-opening stress (S_0) as a function of crack length and load history. The detail for the calculation of cracking-opening stress can be found in ref [**12**].

Once the crack-opening stress is determined, the effective stress intensity range can be calculated. The linear-elastic effective stress intensity range developed by Elber [**13**] is

$$\Delta K_{eff} = (S_{\max} - S_0)\sqrt{(\pi c)}F(c/w) \qquad (1)$$

where S_{max} is the maximum stress, S_0 is the crack opening stress, and F is the boundary correction factor. To account for plasticity, the cyclic plastic zone length ω is added to the crack length, c, as illustrated in Figure **A.1**. The cyclic-plastic-zone-corrected effective stress-intensity factor is

$$(\Delta K_p)_{eff} = (S_{\max} - S_0)\sqrt{(\pi d)}F(d/w) \qquad (2)$$

where d = c+ω/4 and F is the cyclic-plastic-zone corrected boundary-correction factor. The cyclic plastic zone is given by

$$\omega = (1 - R_{eff})^2 \rho/4 \qquad (3)$$

where $R_{eff} = S_0/S_{max}$ and the plastic-zone ρ for a crack in a large plate is

$$\rho = c\{\sec[\pi S_{max}/(2\alpha\sigma_0)] - 1\} \quad (4)$$

where α is a constraint factor and σ_0 is the flow stress.

Consequently, the cyclic plastic zone corrected effective stress intensity range is used to predict crack growth rate, as follows:

$$dc/dN = C(\Delta K_{eff})^n G/H \quad (5)$$

where $G = 1-(\Delta K_0/\Delta K_{eff})^p$ and $H = 1-(K_{max}/C_5)^q$. The function G accounts for threshold variation with stress ratio (since ΔK_0 is a function of stress ratio) and the function H accounts for the rapid crack-growth rates approaching fracture. The parameter C_5 is the cyclic fracture toughness. A discussion of the fracture behaviour is beyond the scope of the present paper, so that H is set to unity. Note that the calculations are performed with FASTRAN Version 4.3.

Figures

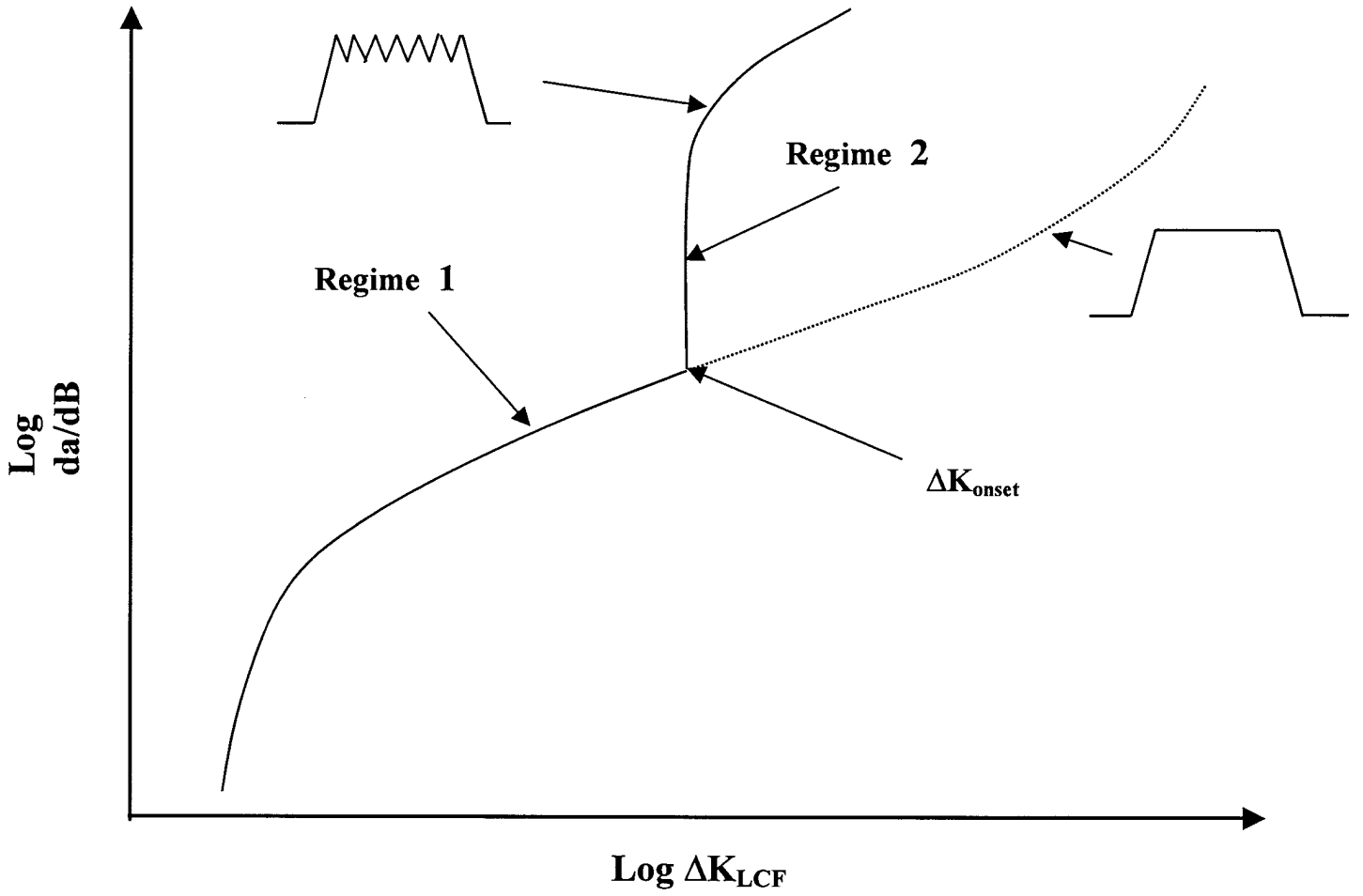

Figure 1 Form of fatigue crack growth rate curve for a simple HCF/LCF loading combination

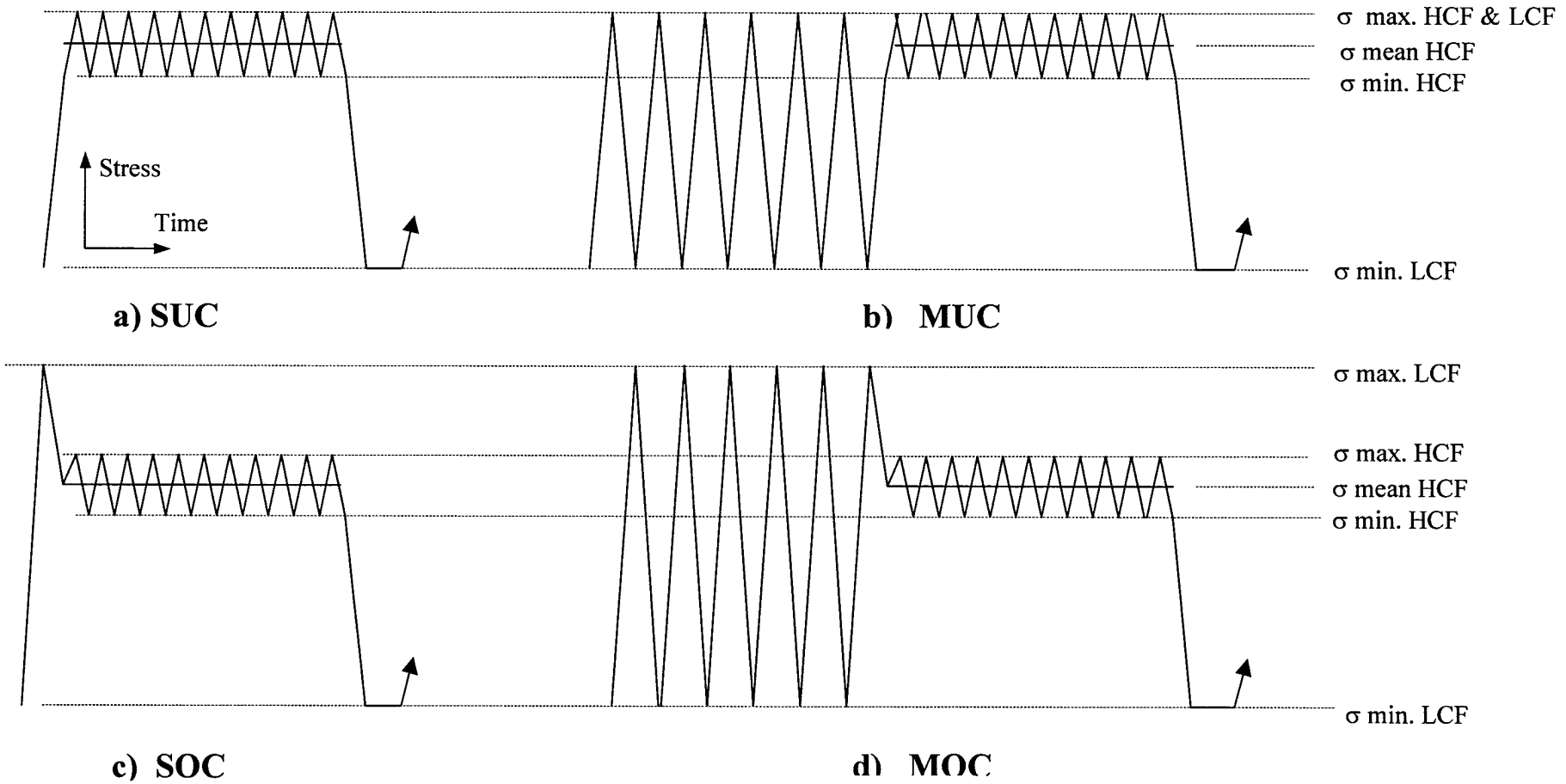

Figure 2 Schematic representations of the repeated stress – time sequences used in the tests. (a) Single Underload Cycle; (b) Multiple Underload Cycles; (c) Single Overload Cycle; (d) Multiple Overload Cycles

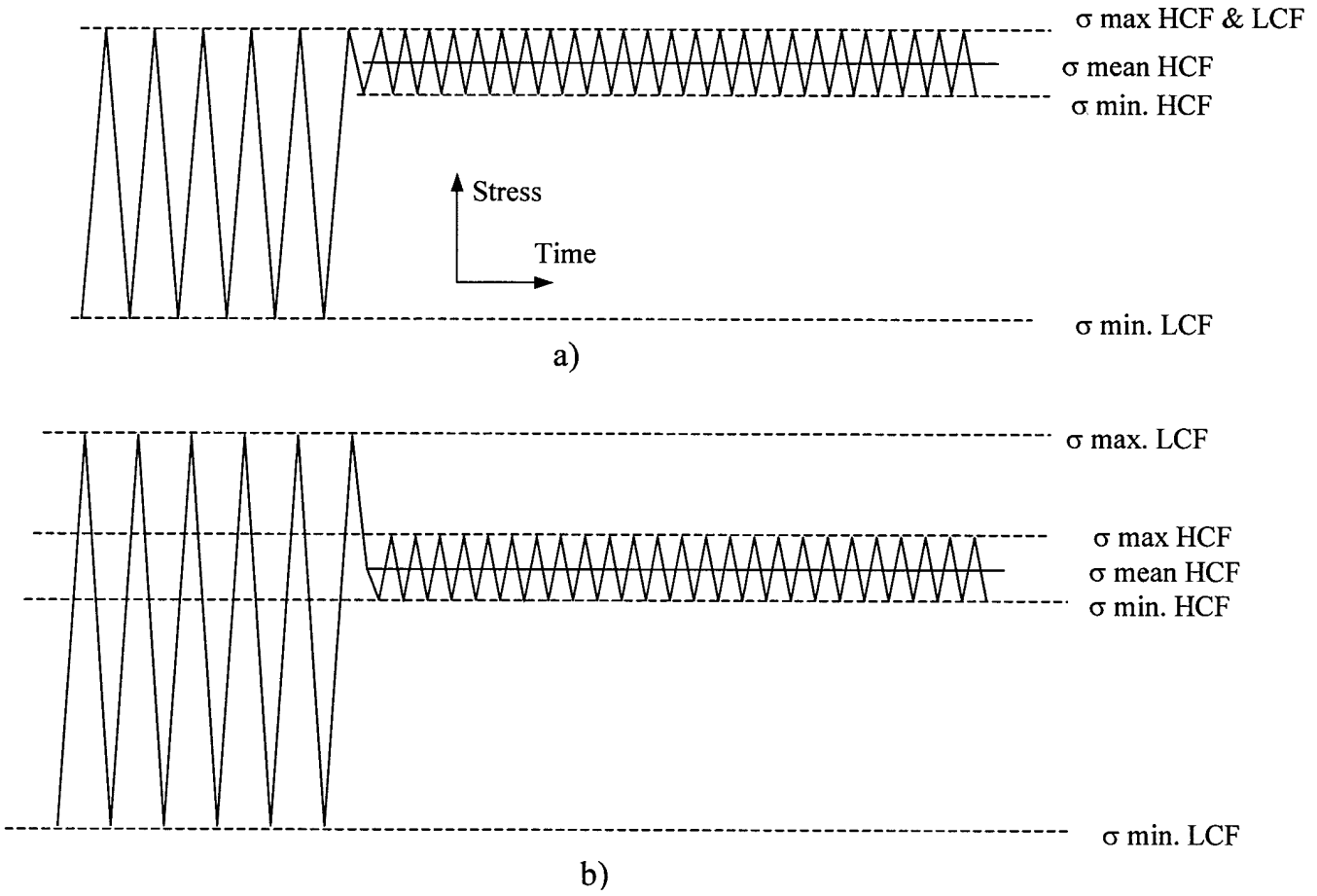

Figure 3 Schematic representation of the stress – time sequences used in the jump-in threshold tests.

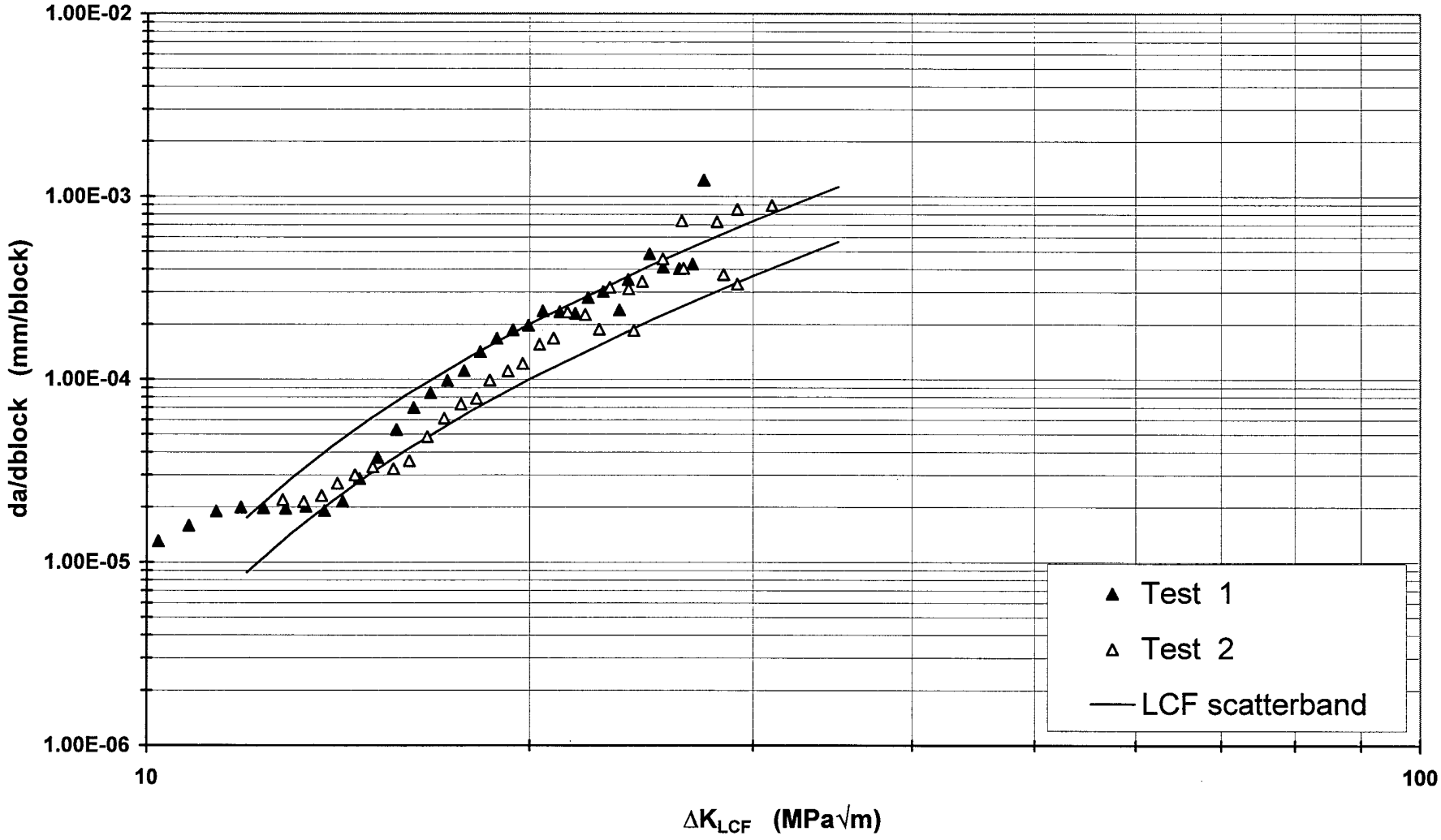

Figure 4 FCG rates without overloads: R_{HCF} = 0.9; T = 1.0; n=1000:1

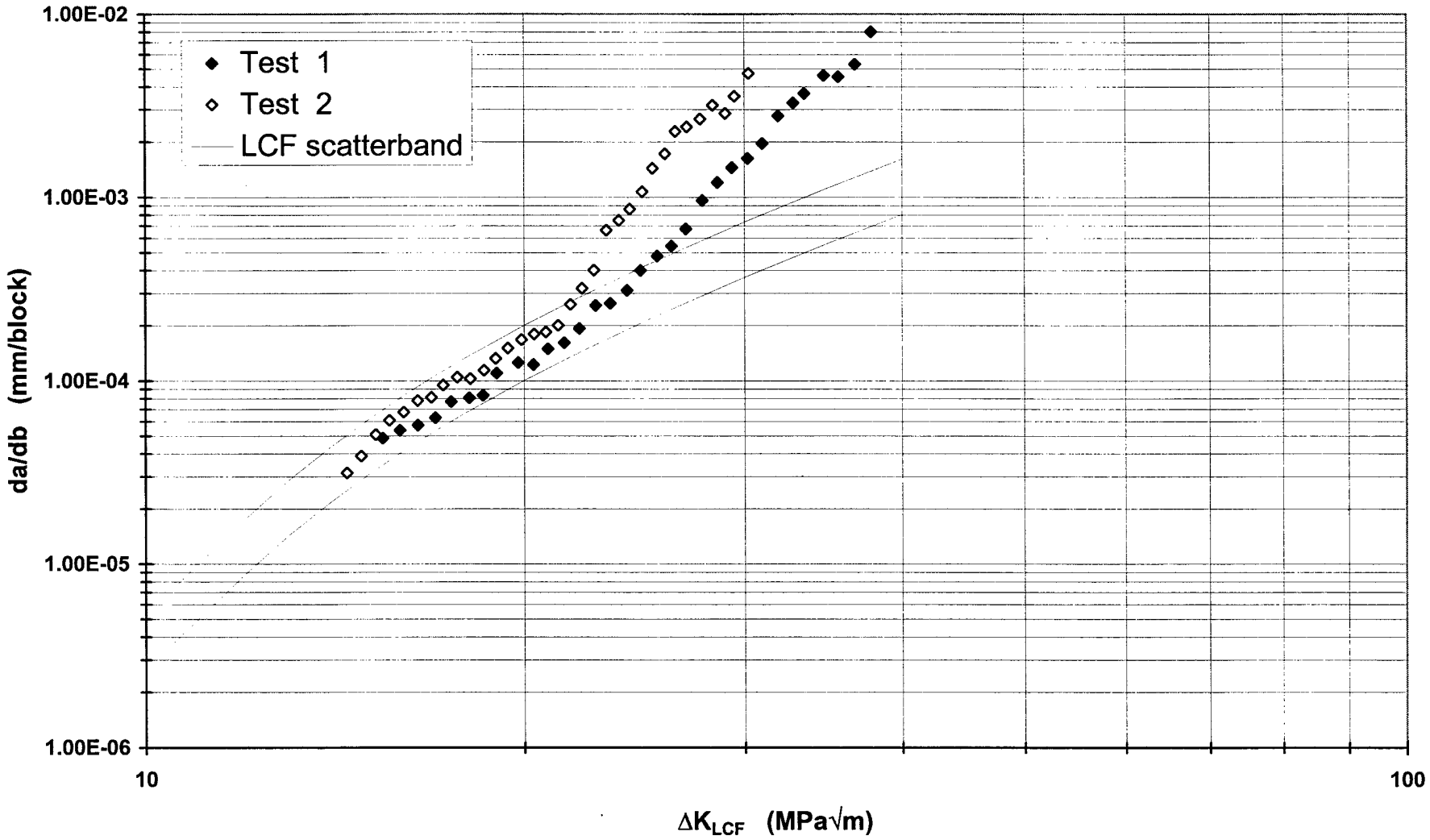

Figure 5 FCG rates without overloads: R_{HCF} = 0.9; T = 1.0; n = 10 000:1

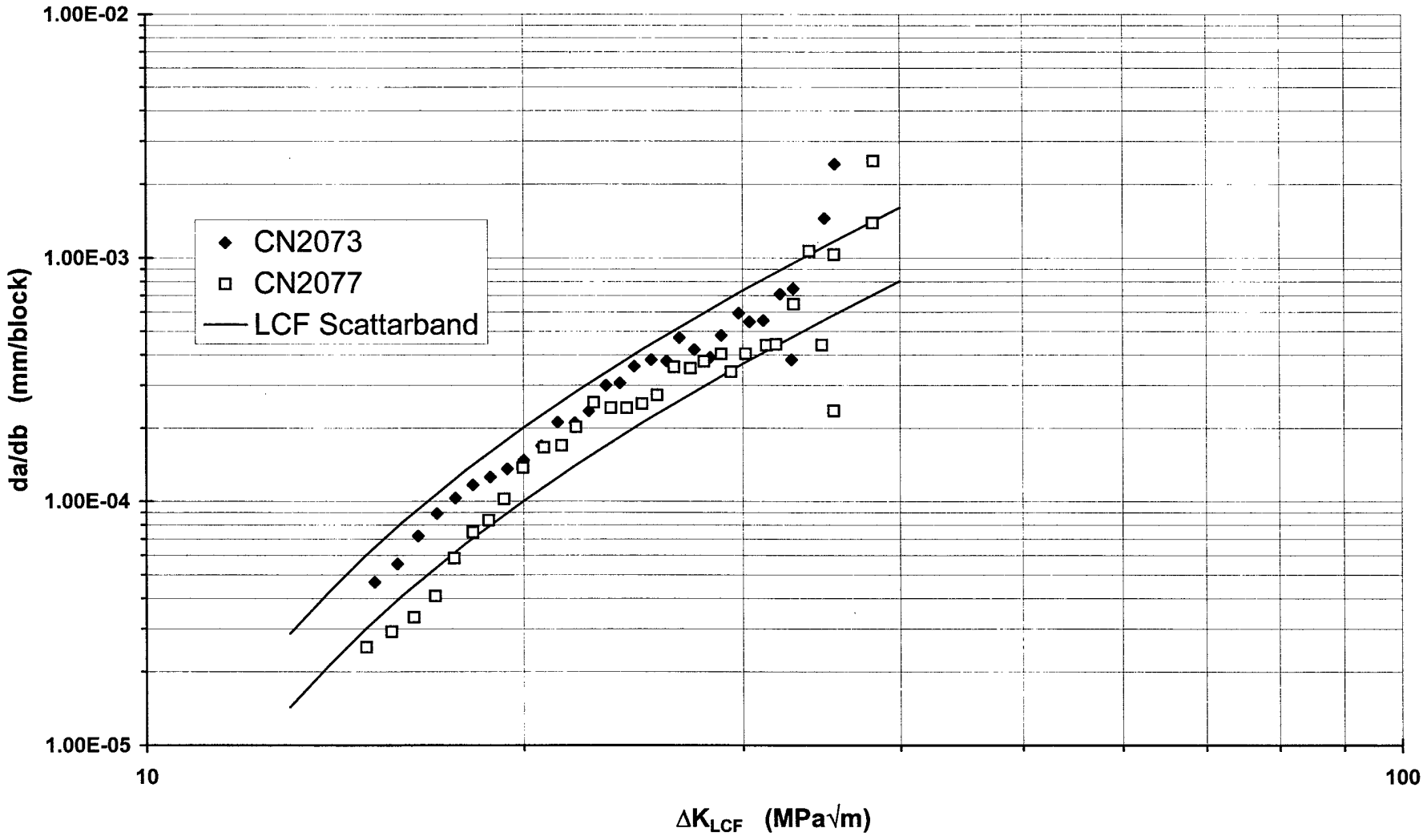

Figure 6 FCG rates with overloads: R_{HCF} = 0.9; T = 1.3, n = 10 000:1

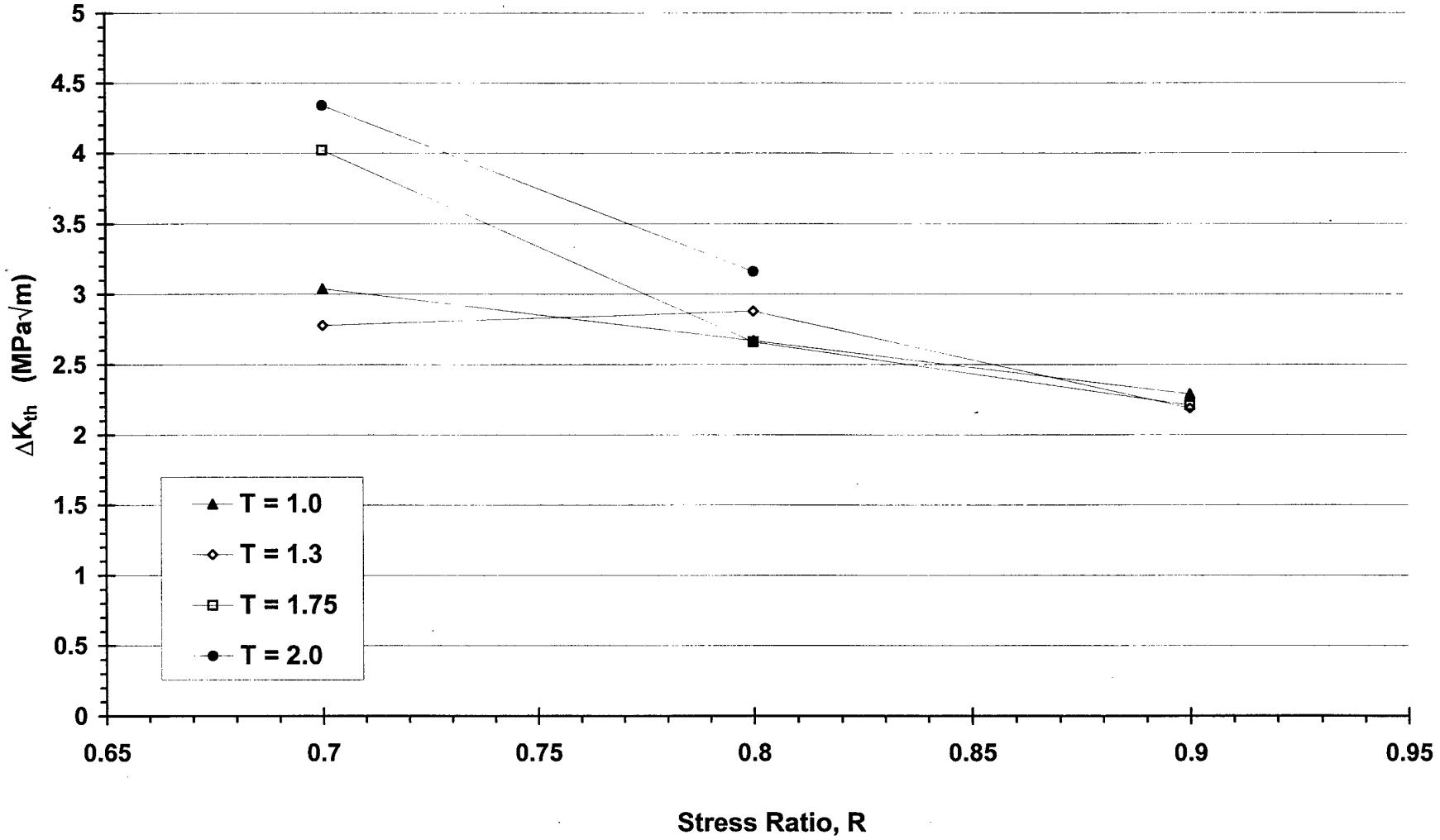

Figure 7 Experimental fatigue threshold values for three stress ratios

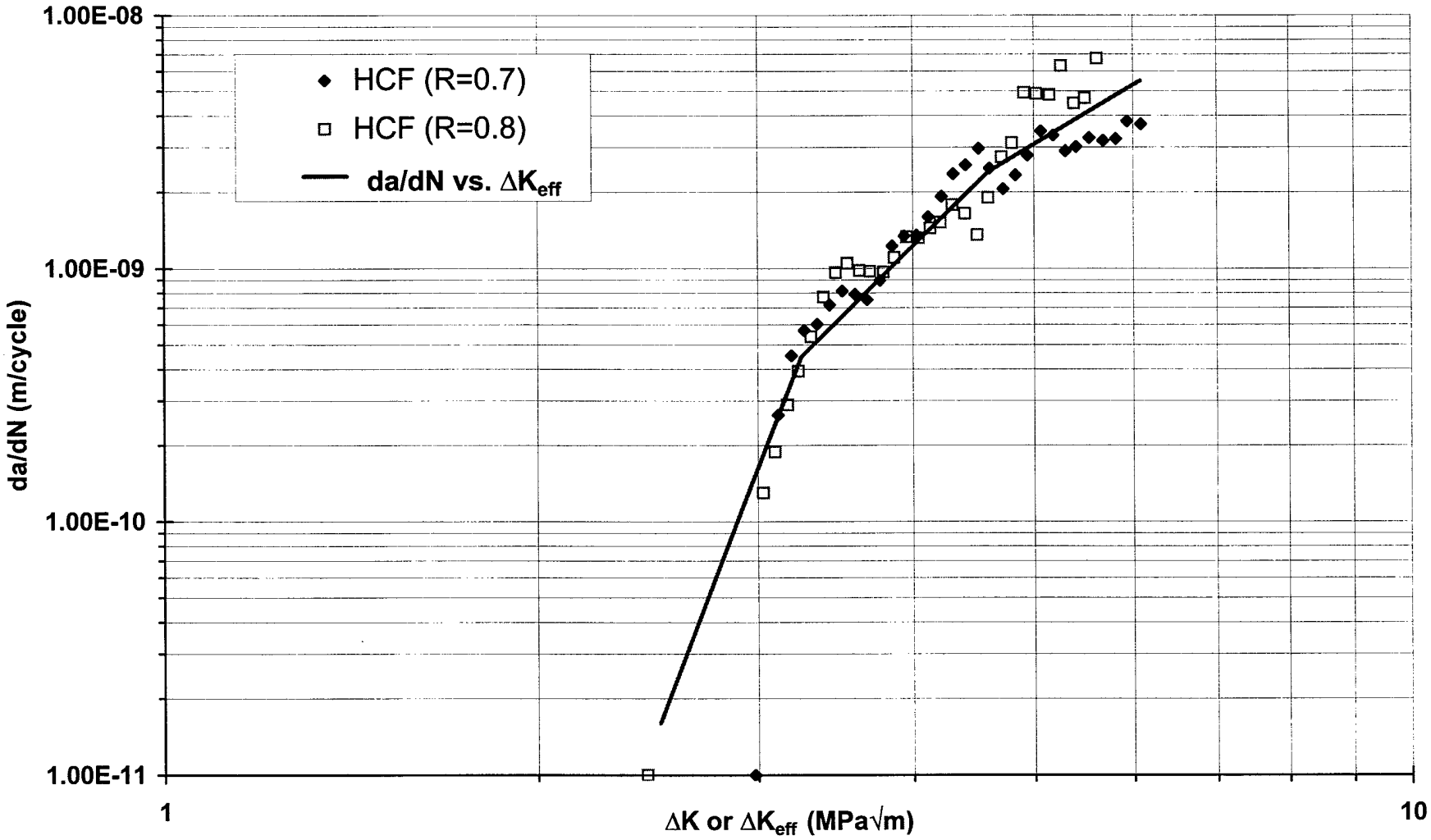

Figure 8 FCG rates against effective stress intensity range curve from experimental constant-amplitude HCF data.

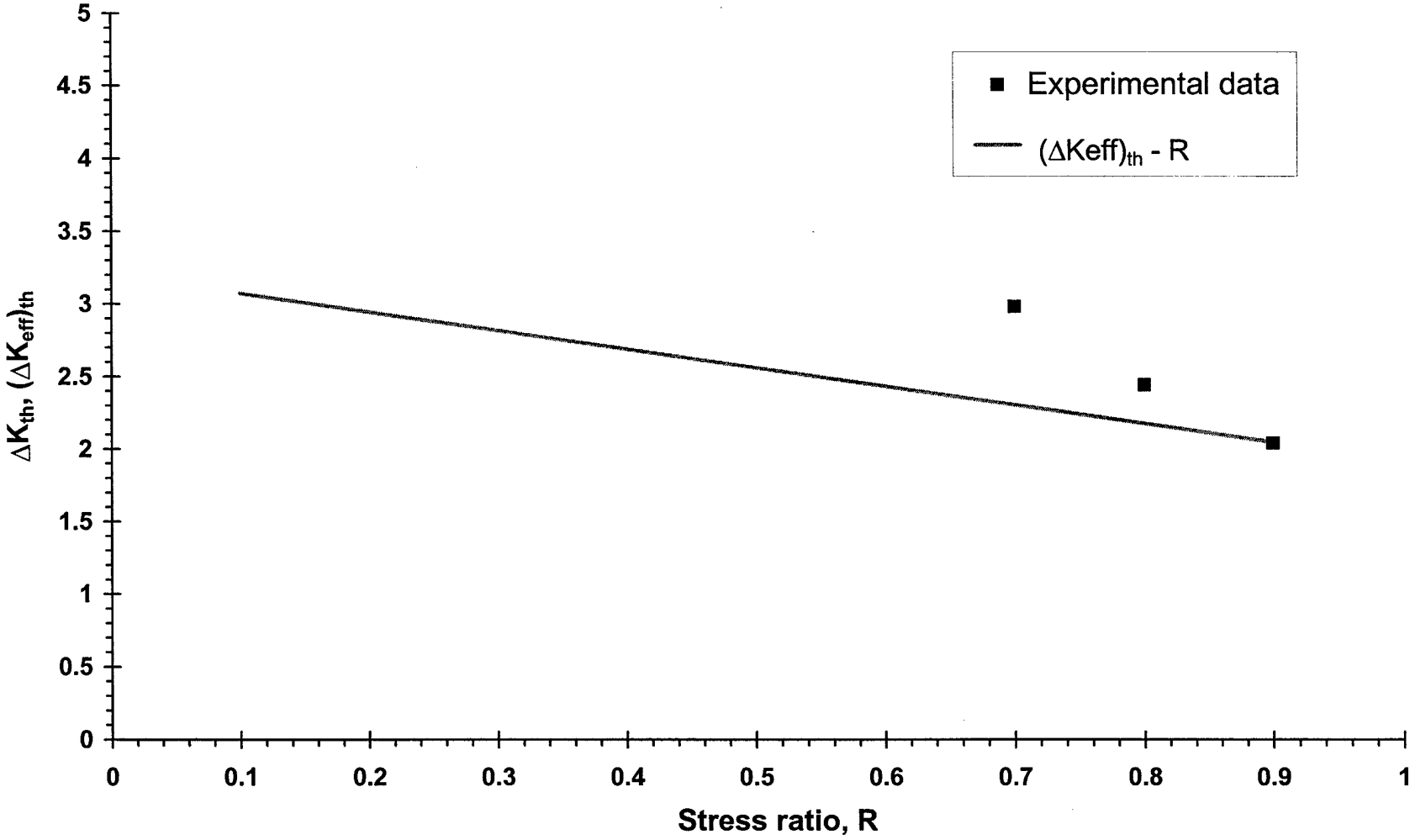

Figure 9 Effective threshold against stress ratio R estimated from experimental threshold data

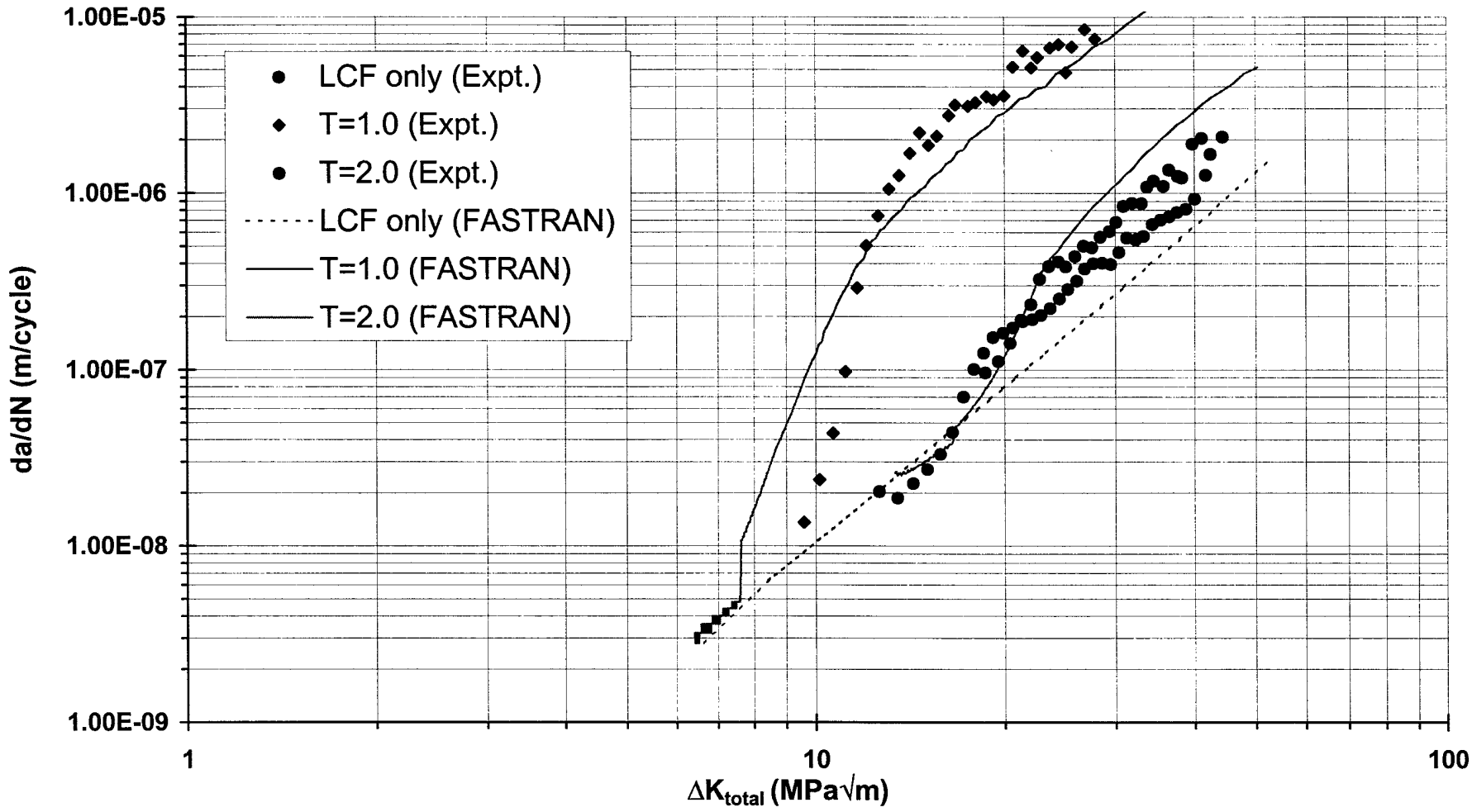

Figure 10 Comparison of predicted and experimental FCG rates under various overload ratios. Stress ratio, R=0.7; cycle ratio =1000:1.

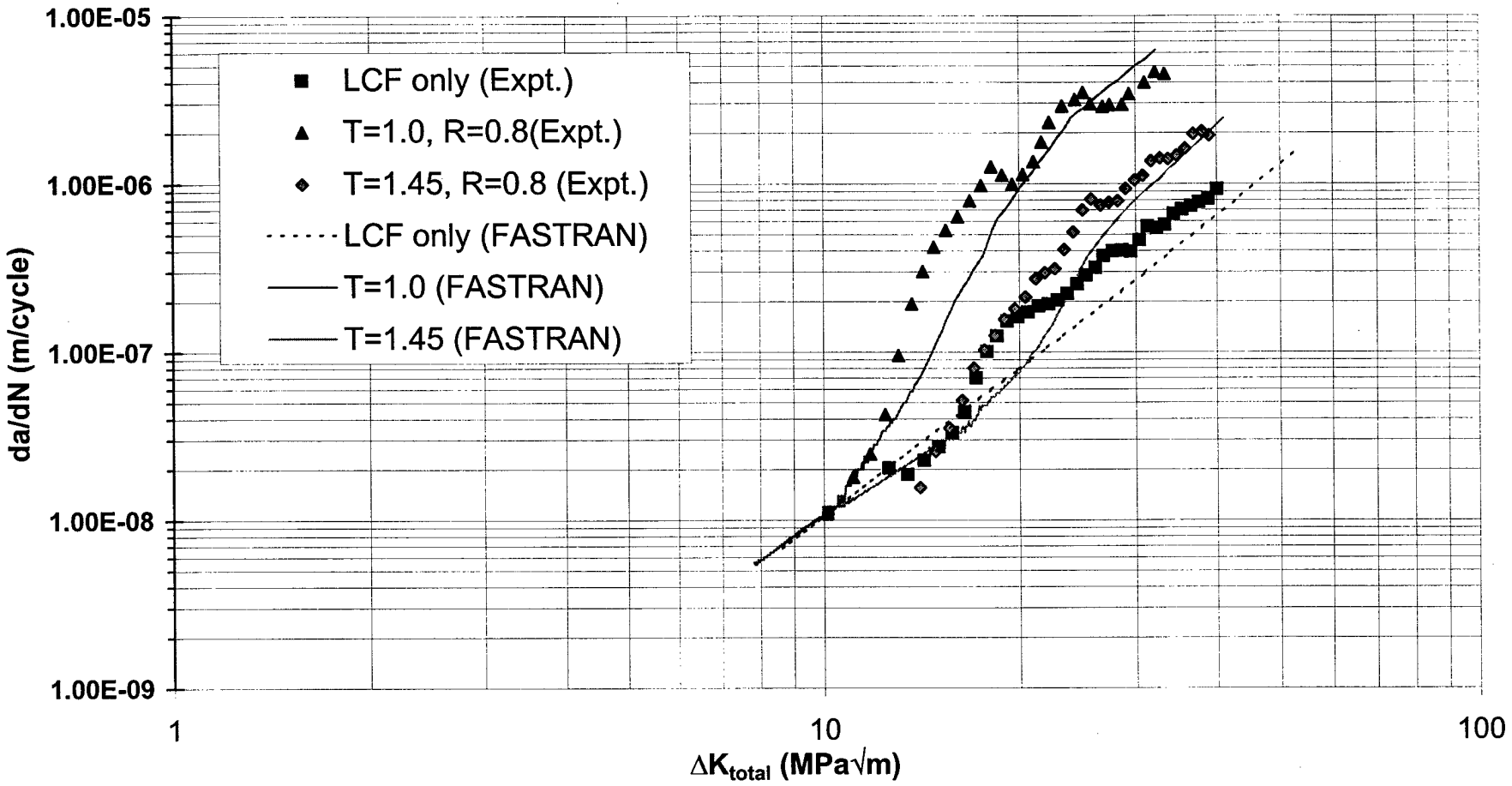

Figure 11 Comparison of predicted and experimental FCG rates under various overload ratios. Stress ratio, R=0.8; cycle ratio =1000:1.

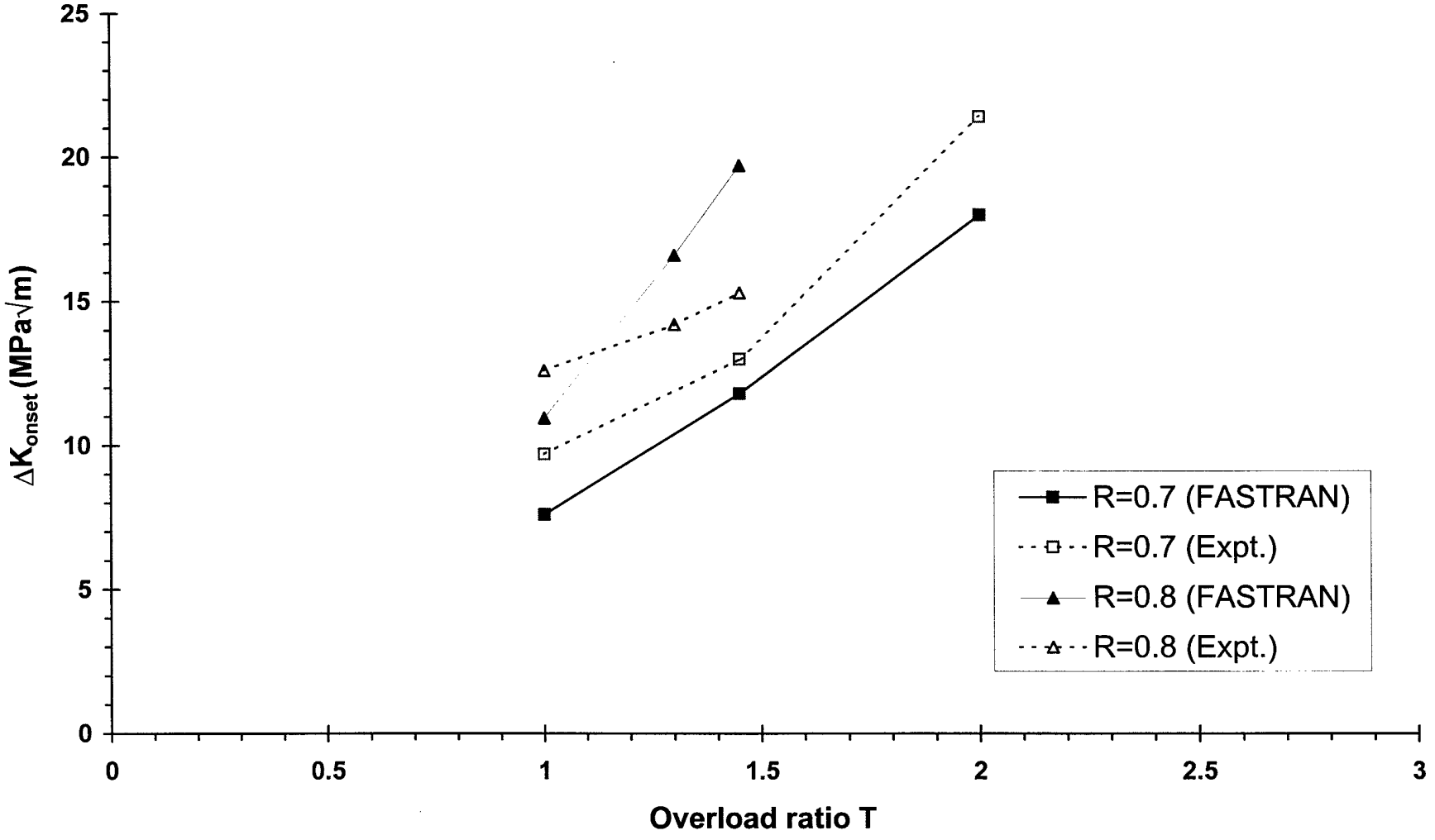

Figure 12 Comparison between the predicted and experimentally measured relationship between ΔK_{onset} and overload ratio T.